Supplemental Figures and Tables:

Structural mechanism of cytosolic DNA sensing by cGAS

Filiz Civril, Tobias Deimling, Carina Mann, Andrea Ablasser, Manuela Moldt, Gregor Witte, Veit Hornung, Karl-Peter Hopfner

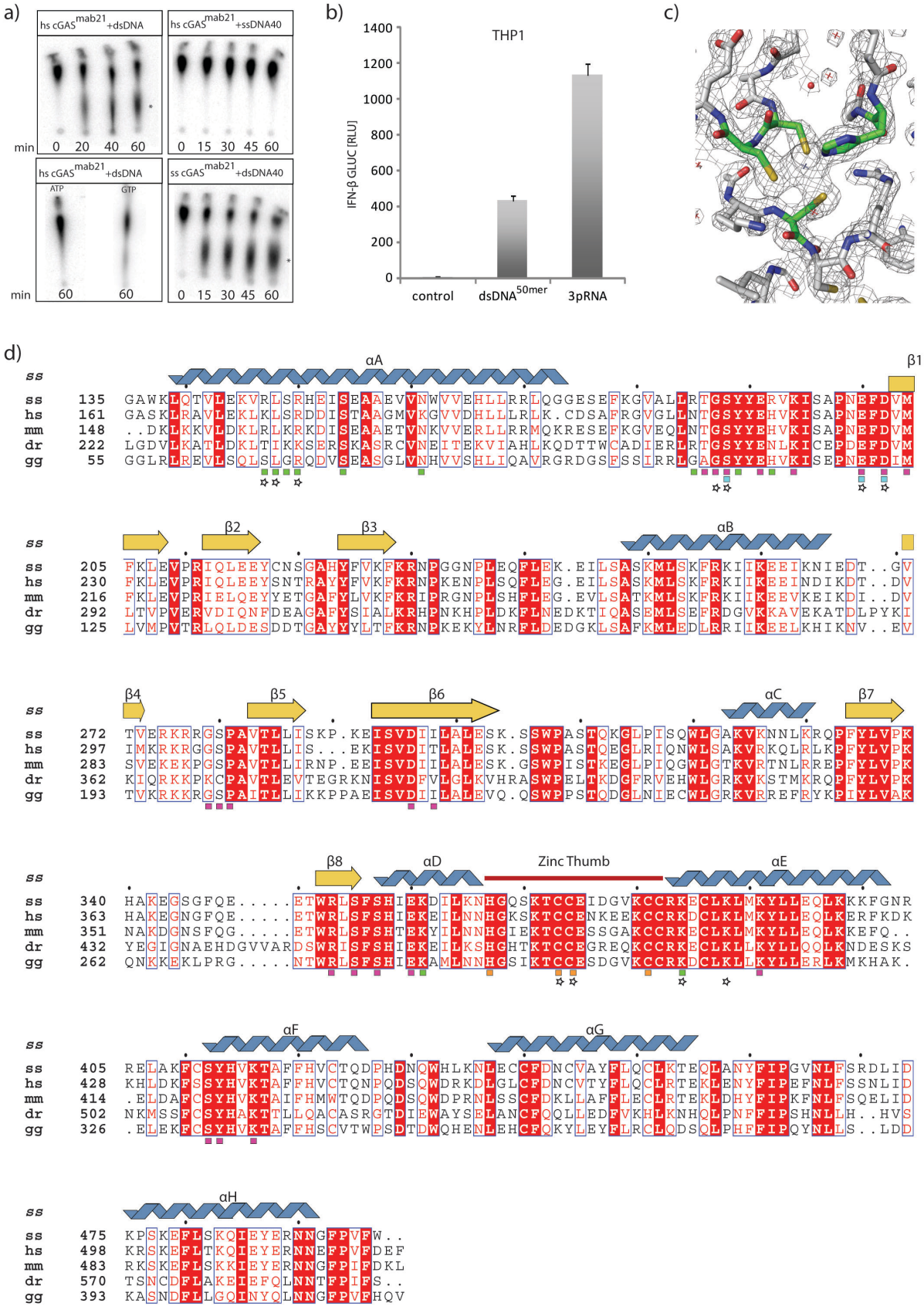
a)
hs cGAS^mab21 +dsDNA
hs cGAS^mab21 +ssDNA40
min
0 20 40 60
0 15 30 45 60
hs cGAS^mab21 +dsDNA
ss cGAS^mab21 +dsDNA40
ATP
GTP
min
60 60
0 15 30 45 60
b)
THP1
IFN-β GLUC [RLU]
1400
1200
1000
800
600
400
200
0
control
dsDNA^50mer
3pRNA
c)
d)
αA
β1
β2
β3
αB
β4
β5
β6
αC
β7
β8
αD
Zinc Thumb
αE
αF
αG
αH
ss
ss 135 GAWKLQTVLEKVRLSRHEISEAAEVVNWVVEHLLRRLQGGESEFKGVALLRTGSYYERVKISAPNEFDVM
hs 161 GASKLRAVLEKLKLSRDDISTAAGMVKGVVDHLLLRLK.CDSAFRGVGLLNTGSYYEHVKISAPNEFDVM
mm 148 ..DKLKKVLDKLRLKRKDISEAAETVNKVVERLLRRMQKRESEFKGVEQLNTGSYYEHVKISAPNEFDVM
dr 222 LGDVLKATLDKLTIKKSERSKASRCVNEITEKVIAHLKQDTTWCADIERLRTGSYYENLKICEPDEFDVM
gg 55 GGLRLREVLSQLSLGRQDVSEASGLVNHVVSHLIQAVRGRDGSFSSIRRLGAGSYYEHVKISEPNEFDIM
ss 205 FKLEVPRIQLEEYCNSGAHYFVKFKRNPGGNPLEQFLEK.EILSASKMLSKFRKIKEEIKNIEDT..GV
hs 230 FKLEVPRIQLEEYSNTRAYYFVKFKRNPKENPLSQFLEG.EILSASKMLSKFRKIKEEINDIKDT..DV
mm 216 FKLEVPRIELQEYYETGAFYLVKFKRIPRGNPLSHFLEG.EVLSATKMLSKFRKIIKEEVKEIKDI..DV
dr 292 LTVPVERVDIQNFDEAGAFYSIALKRHPNKHPLDKFLNEDKTIQASEMLSEFRDGVKKAVEKATDLPYKI
gg 125 LVMPVTRLQLDESDDTGAYYYLTFKRNPKEKYLNRFLDEDGKLSAFKMLEDLRRIIKEELKHIKNV..EV
ss 272 TVERKRRGSPAVTLLISKP.KEISVDIILALESK.SSWPASTQKGLPISQWLGAKVKNNLKRQPFYLVPK
hs 297 IMKRKRGGSPAVTLLIS...EKISVDITLALESK.SSWPASTQEGLRIQNWLSAKVRKQLRLKPFYLVPK
mm 283 SVEKEKPGSPAVTLLIRNP.EEISVDIILALESK.GSWPISTKEGLPIQGWLGTKVRTNLRREPFYLVPK
dr 362 KIQRKKPKCPAVTLEVTEGRKNISVDFVLGLKVHRASWPELTKDGFRVEHWLGRKVKSTMKRQPFYLVPK
gg 193 TVKRKKRGSPAITLLIKKPPAEISVDIILALEVQ.QSWPPSTQDGLNIECWLGRKVRREFRYKPIYLVAK
ss 340 HAKEGSGFQE.....ETWRLSFSHIEKDILKNHGQSKTCCEIDGVKCCRKECLKLMKYLLEQLKKKFGNR
hs 363 HAKEGNGFQE.....ETWRLSFSHIEKEILNNHGKSKTCCENKEEKCCRKDCLKLMKYLLEQLKERFKDK
mm 351 NAKDGNSFQG.....ETWRLSFSHTEKYILNNHGIEKTCCESSGAKCCRKECLKLMKYLLEQLKKEFQ..
dr 432 YEGIGNAEHDGVVARDSWRISFSHIEKEILKSHGHTKTCCEGREQKCCRKECLKLLKYLLQQLKNDESKS
gg 262 QNKKEKLPRG.....NTWRLSFSHIEKAMLNNHGSIKTCCESDGVKCCRKDCLKLLKYLLERLKMKHAK.
ss 405 RELAKFCSYHVKTAFFHVCTQDPHDNQWHLKNLECCFDNCVAYFLQCLKTEQLANYFIPGVNLFSRDLID
hs 428 KHLDKFSSYHVKTAFFHVCTQNPQDSQWDRKDLGLCFDNCVTYFLQCLRTEKLENYFIPEFNLFSSNLID
mm 414 .ELDAFCSYHVKTAIFHMWTQDPQDSQWDPRNLSSCFDKLLAFFLECLRTEKLDHYFIPKFNLFSQELID
dr 502 NKMSSFCSYHAKTTLLQACASRGTDIEWAYSELANCFQQLLEDFVKHLKNHQLPNFFIPSHNLLH..HVS
gg 326 .ELEKFCSYHVKTAFFHSCVTWPSDTDWQHENLEHCFQKYLEYFLRCLQDSQLPHFFIPQYNLLS..LDD
ss 475 KPSKEFLSKQIEYERNNGFPVFW..
hs 498 KRSKEFLTKQIEYERNNEFPVFDEF
mm 483 RKSKEFLSKKIEYERNNGFPIFDKL
dr 570 TSNCDFLAKEIEFQLNNTFPIFS..
gg 393 KASNDFLLGQINYQLNNGFPVFHQV

Supplemental Figure S1: Activity assays, electron density and cGAS sequence alignment

a) Activity assays with human and porcine $cGAS^{mab21}$ in the presence of ATP, GTP and ATPα^{32}P. Upper panel left: 2µM human $cGAS^{Mab21}$ + dsDNA (50mer), right: 1µM human $cGAS^{Mab21}$ + 0.5µM ssDNA (40mer). Lower panel left: 2µM human $cGAS^{Mab21}$ + 3µM dsDNA (50mer) using only ATP/ATPα^{32}P and only GTP/GTPα^{32}P, respectively; right: 1µM porcine $cGAS^{Mab21}$ + 0.5µM dsDNA (40mer). The reactions were stopped at indicated time points by plotting on TLC plates. Both human and porcine $cGAS^{Mab21}$ are activated by dsDNA while ssDNA and single nucleotides fail to induce activity.

b) IFN-β stimulation in THP1 cells by $dsDNA^{50mer}$ or with 5'triphosphate dsRNA (3pRNA). 200ng of indicated ligand was transfected to THP1 cells along with IFN-β promoter reporter plasmid pIFN-β-GLUC. Luciferase activity is plotted: mean ± sd (n=3). The $dsDNA^{50mer}$ used in *in vitro* assays induces interferon production in THP1 cells. 3pRNA, which induces the RIG-I pathway, is used as positive control. The negative control is without ligand.

c) $2F_o$-F_c electron density overlaid with the final model around the thumb (carbons green). The $2F_o$-F_c map is contoured at 2σ.

d) Structure based alignment of selected $cGAS^{Mab21}$ sequences (abbreviations: *Sus scrofa*: **ss**, *Homo sapiens*: **hs**, *Mus musculus*: **mm**, *Danio rerio*: **dr**, *Gallus gallus*: **gg**) with highlighted conserved residues and annotated motifs. The secondary structural elements are shown on top of the alignment for the porcine homolog, color coding is analogous to Fig. 1. The squares mark residue contacts: green => DNA, magenta => GTP/ATP, cyan => Mg^{2+}, orange => Zn^{2+}. Stars denote residues that are mutated in this study.

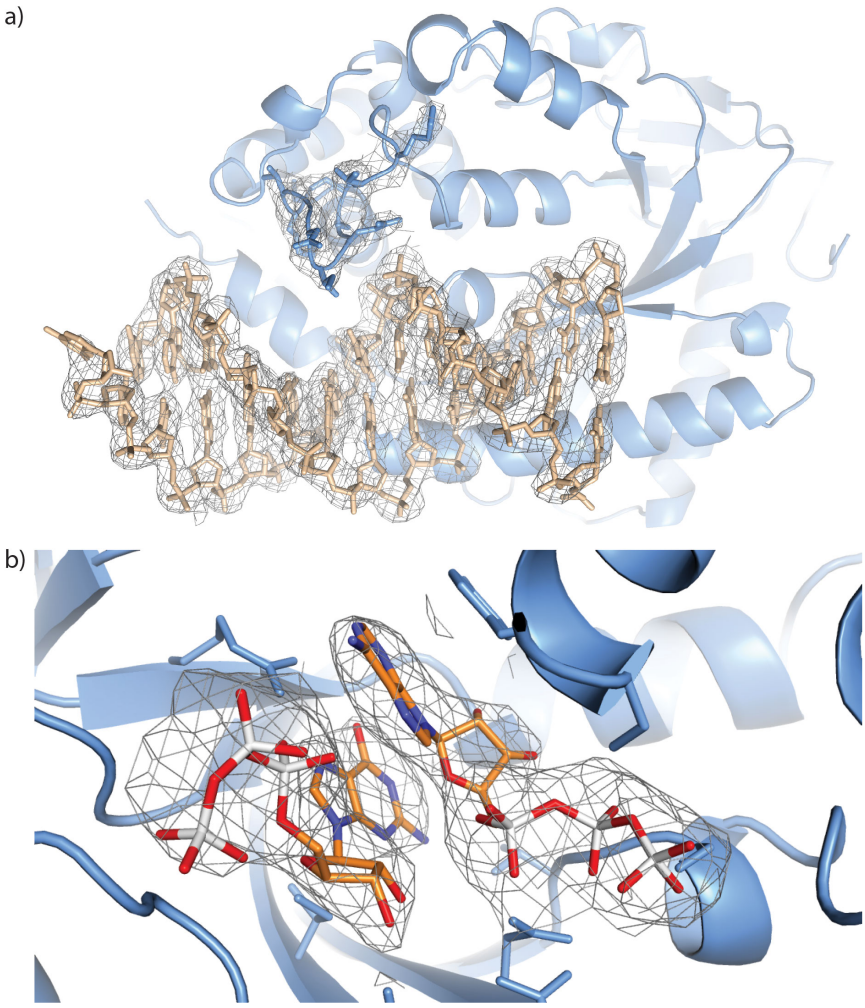

Supplemental Figure S2: Electron densities

a) Ribbon model of cGAS$^{Mab21(td)}$ (blue) with bound dsDNA (beige stick representation). $2F_o$-F_c electron density for the DNA and the Zn-thumb residues are shown at a contour level of 1σ.

b) $2F_o$-F_c electron density around the two nucleotides in the active site (contour level of 1σ).

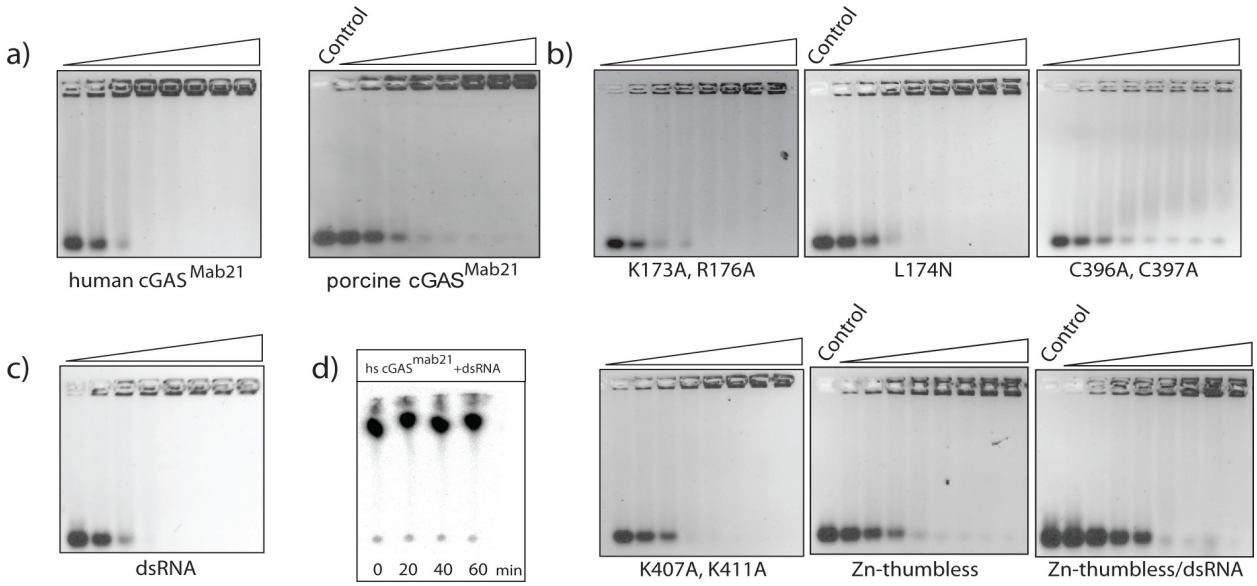

Supplementary Figure S3: Electrophoretic mobility shift and activity assays

a) Electrophoretic mobility shift analysis of dsDNA^{50mer} (0.2 µM) with human or porcine cGAS^{Mab21} (protein concentrations are 0.5, 0.75, 1.00, 1.25, 1.50, 1.75, 2.00, 2.50 µM (triangle)). Control: without protein.

b) Like a), but with human cGAS^{Mab21} mutants.

c) Like a) but binding of human cGAS^{Mab21} to dsRNA^{50mer}.

d) Activity assay with 2µM human cGAS^{Mab21} + 3µM dsRNA^{50mer}.

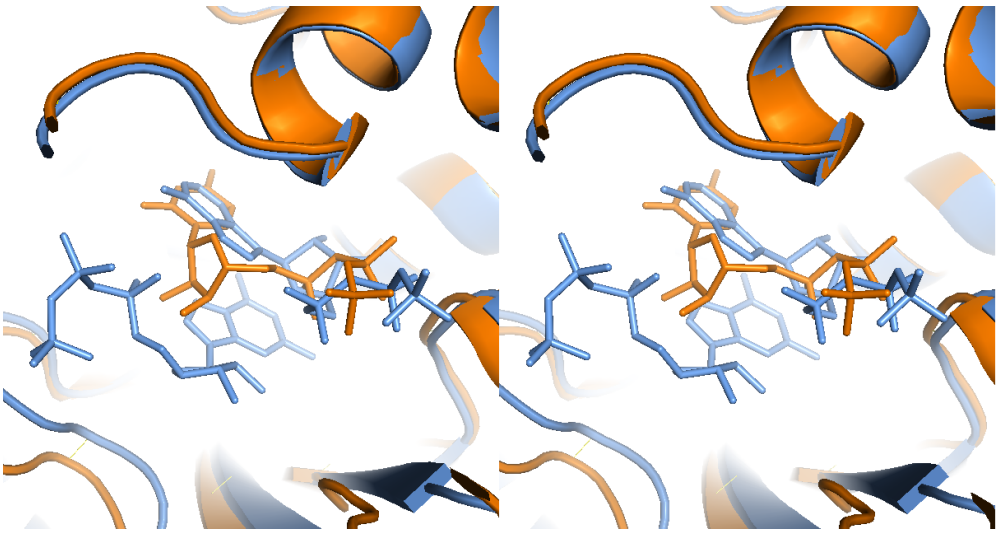

Supplementary Figure S4: Comparison of UTP- and ATP/GTP-bound structure of cGAS^{Mab21}

The stereo figure shows the active site of the superimposed structures of the UTP-bound state of cGAS^{Mab21} (orange) and the cGAS$^{Mab21(td)}$:DNA:GTP:ATP complex (blue), respectively. The ribose moiety is flipped in UTP as compared to ATP.

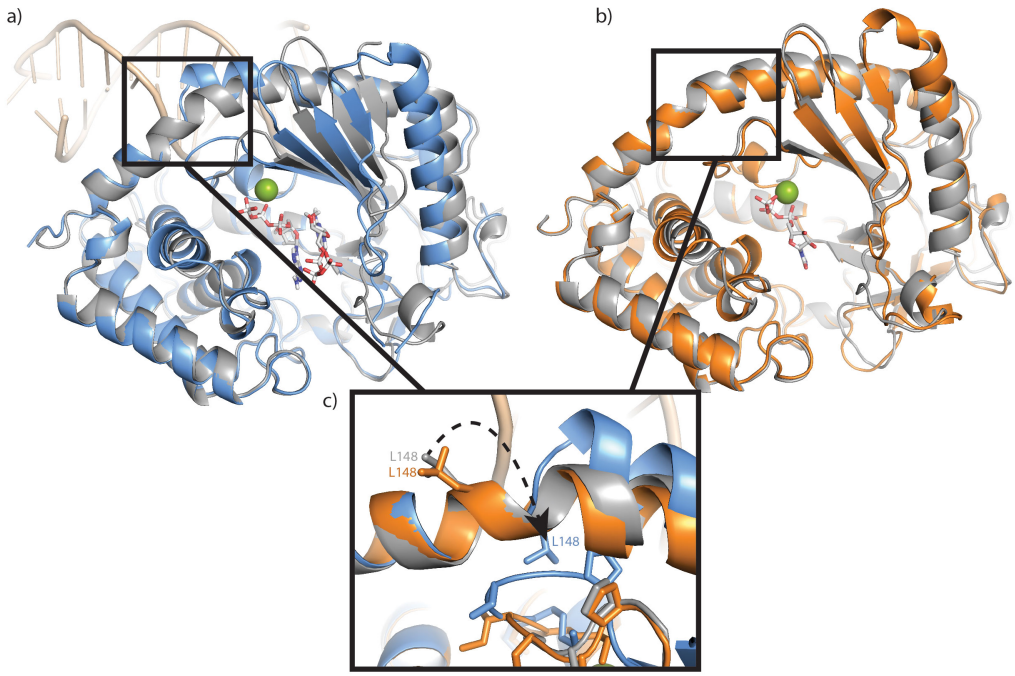

Supplementary Figure S5: Comparison of cGAS^{Mab21} structures

a) Superposition of the DNA-bound (blue) and apo (grey) cGAS^{Mab21} structures.

b) Superposition of apo (grey) cGAS^{Mab21} and UTP-bound (orange) cGAS^{Mab21}.

c) The Leu148 flip upon DNA binding. In the absence of DNA (orange UTP-bound and grey apo structures) Leu148 is solvent exposed. In the DNA binding conformation (blue), Leu148 flips and helps stabilize the nucleotide-binding loop.

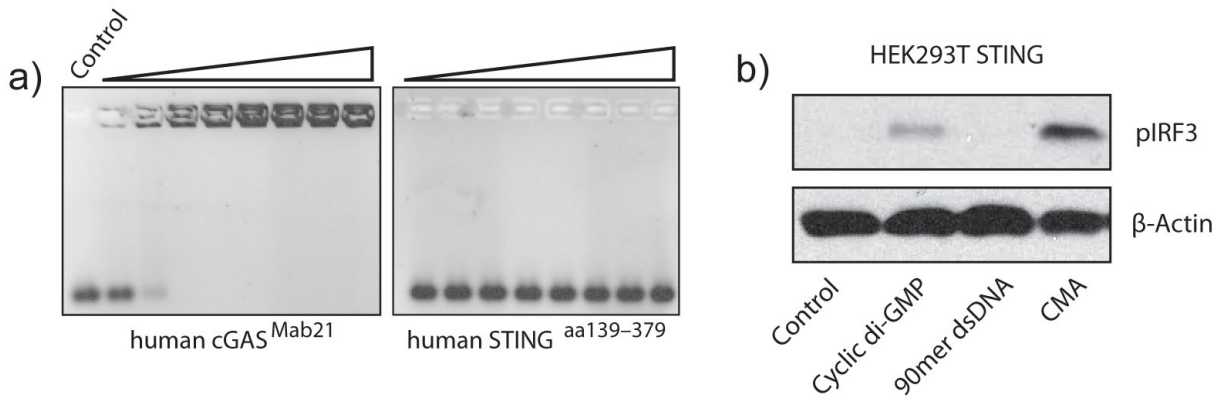

Supplementary Figure S6: Comparison of STING and cGAS DNA binding and STING in vivo activity.

a) Electrophoretic mobility shift analysis of dsDNA (0.2 µM) with human cGAS^{Mab21} (left) and human STING$^{aa139-379}$ (right) (protein concentrations are 0.5, 1.0, 2.0, 3.0, 5.0, 7.0, 10, 15 µM, control: without protein). While human cGAS^{Mab21} readily binds dsDNA at a concentration as low as 0.5 µM, human STING$^{aa139-379}$ fails binding even at concentration as high as 15 µM.

b) Western blot analysis of IRF3 phosphorylation which indicates interferon stimulation. The HEK293T cells stably expressing STING were induced with cyclic-di-GMP, dsDNA^{90mer} and 10-carboxymethyl-9-acridanone (CMA). The proven STING ligands cyclic-di-GMP and CMA induce IRF3 phosphorylation while DNA^{90mer} fails, suggesting requirement of a sensor that detects DNA upstream of STING. β-actin was used as loading control.

Supplemental Table S1 Data collection and refinement statistics

	SeMet	Apo	+UTP	DNA-GTP-ATP complex
Data collection				
Space group	$C222_1$	$C222_1$	$P2_12_12_1$	$C222_1$
Cell dimensions				
a, *b*, *c* (Å)	47.5, 119.9, 140.9	47.4, 118.0, 142.6	80.6, 97.7, 107.0	86.2, 111.7, 117.6
α, β, γ (°)	90, 90, 90	90, 90, 90	90, 90, 90	90, 90, 90
Resolution (Å)	47.1 (2.5)*	47.5 (2.0)*	46.9 (2.28)*	999.0 (3.1)*
R_{merge}	9.0 (44.7)*	4.7 (57.5)*	5.8 (59.1)*	9.0 (90.7)*
$I / \sigma I$	13.8 (3.3)*	20.9 (2.6)*	12.0 (2.0)*	17.0 (1.9)*
Completeness (%)	98.7 (92.0)*	99.6 (98.4)*	95.9 (93.3)*	98.6 (91.7)*
Redundancy	6.8 (6.4)*	6.4 (5.9)*	2.3 (2.3)*	6.9 (6.6)*
Wavelength (Å)	0.97961	1.00665	0.97934	0.97626
Refinement				
Resolution (Å)		45.5 - 2.0	44.6 - 2.27	68.3 - 3.08
No. reflections		51611	72224	10739
R_{work} / R_{free} (%)		18.6 / 21.3	17.0 / 20.4	25.5 / 25.8
No. atoms				
Protein		2878	5969	2899
DNA		-	-	555
Ligand/ion		54	62	73
Water		132	306	2
B-factors				
Protein		52.2	38.0	101.4
DNA		-	-	113.6
Ligand/ion		65.6	41.5	129.5
Water		45.1	38.2	95.59
R.m.s. deviations				
Bond lengths (Å)		0.008	0.009	0.004
Bond angles (°)		1.07	1.19	0.888
Ramachandran (%)				
Favored		97.4	98.6	96.0
Allowed		2.3	1.4	4.0
Outliers		0.3	0	0
PDB Accession Code		4JLX	4JLZ	4KB6

*Values in parentheses are for the highest-resolution shell.